Extreme ultraviolet mask roughness: requirements, characterization, and modeling

Patrick Naulleau,[1] Suchit Bhattaria, Rick Chao,[2] Rene Claus,[2] Kenneth Goldberg,[1] Frank Goodwin,[3] Eric Gullikson,[1] Donggun Lee,[4] Andy Neureuther,[2] and Jong-Ju Park[4]

1) Center for X-Ray Optics, Lawrence Berkeley National Laboratory, Berkeley, CA 94720
2) University of California, Berkeley, Berkeley, CA 94720
3) SEMATECH, Albany, NY 12203
4) Samsung Electronics, Hwasung-City, Gyeonggi-Do, Korea 445-701

ABSTRACT

It is now well established that extremely ultraviolet (EUV) mask multilayer roughness can lead to wafer-plane line-edge roughness (LER) in lithography tools. It is also evident that this same effect leads to sensor plane variability in inspection tools. This is true for both patterned mask and mask blank inspection. Here we evaluate mask roughness specifications explicitly from the actinic inspection perspective. The mask roughness requirement resulting from this analysis are consistent with previously described requirements based on lithographic LER.

In addition to model-based analysis, we also consider the characterization of multilayer mask roughness and evaluate the validity of using atomic force microscopy (AFM) based measurements by direct comparison to EUV scatterometry measurements as well as aerial image measurements on a series of high quality EUV masks. The results demonstrate a significant discrepancy between AFM results and true EUV roughness as measured by actinic scattering.

Keywords: extreme ultraviolet, lithography, line-edge roughness, multilayer, speckle, photomask, surface roughness

1. INTRODUCTION

The extremely short wavelength and reflective nature of extreme ultraviolet (EUV) lithography renders it much more susceptible to surface roughness than is deep ultraviolet (DUV) lithography. Considering the phase error imparted to the wavefront by the optical surface, we see that EUV is nearly 100× more sensitive to surface roughness than DUV. For imaging optics, this translates to increased flare and much effort has been directed at reducing roughness to mitigate flare [1]. For optical components conjugate to the image plane (such as the mask), however, roughness does not lead to flare, but rather to speckle and ultimately line edge/width roughness (LER/LWR) in the lithography process [2-4]. Based on ITRS requirements [5] and assumed error budgets, LER-limited patterning process window analysis has shown the EUV mask roughness requirement to be on the order of 50 pm [6]. Mask roughness, however, also has implications on defectivity and actinic inspection. In this paper we consider these additional impacts and their implications on mask roughness requirements. Finally we consider mask roughness metrology and demonstrate the validity of the roughness imaging models by direct comparison to EUV aerial image microscopes.

EUV roughness on the mask can come from three primary sources, substrate roughness replicated through the multilayer [6], coating induced roughness [7], and capping layer roughness [8]. Replicated substrate roughness is the most severe since it geometrically maps to EUV phase roughness with an additional factor of 2 due to the reflection. Coating induced roughness maps to both reflected phase and amplitude variations by way of the Bragg structure with the coupling depending on the details of the coating process. Capping layer roughness also leads to reflected phase and amplitude variations but by way of refraction and thus is the least severe of the three. Ultimately, all that matters is the total effective EUV roughness. In the analysis to follow, we will ignore the reflected amplitude roughness term and consider the total effective EUV phase roughness reporting it as a reflective surface height variation.

Photomask and Next-Generation Lithography Mask Technology XXI, edited by Kokoro Kato, Proc. of SPIE Vol. 9256, 92560J · © 2014 SPIE
CCC code: 0277-786X/14/$18 · doi: 10.1117/12.2070303

2. THE IMPORTANCE OF DEFOCUS

The coupling of mask roughness to LWR is heavily dependent on defocus. This is because defocus leads to both increased speckle contrast and decreased image log slope (ILS) which determines the extent to which the speckle intensity variations couple to edge displacements. It is instructive to understand the relative importance of these two terms: the plot in Fig. 1(a) shows the computed speckle contrast and the ILS assuming an ideal 0.33 numerical aperture (NA) system imaging 22-nm lines and spaces with disk illumination (partial coherence of 0.7) and an assumed 75-pm of roughness. Figure 1(b) shows the LWR degradation factor relative to the in focus position which is computed by normalizing the RMS speckle contrast and inverse of the ILS, respectively. The results show that for defocus values smaller than one Rayleigh unit [9], the change in speckle contrast is the dominant term.

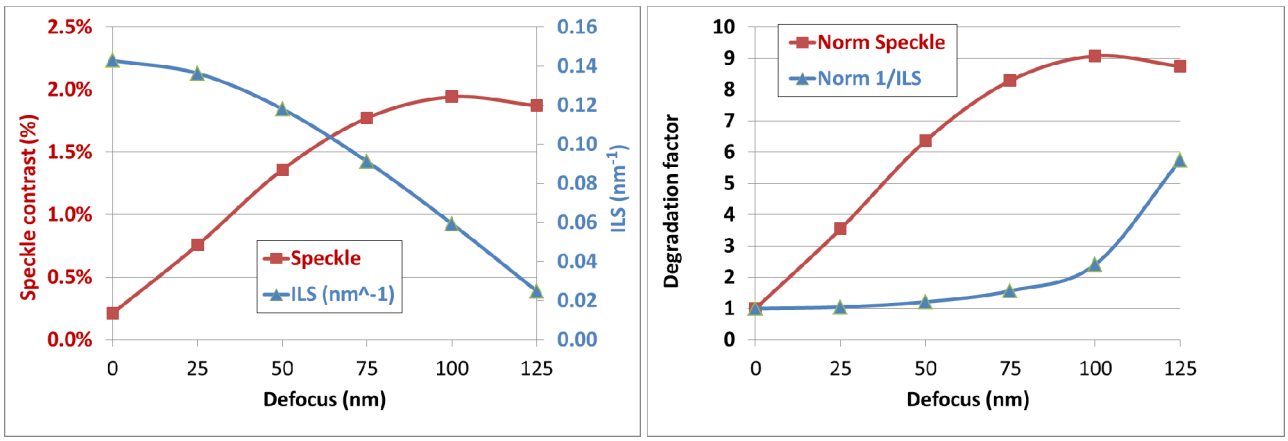

Fig. 1. (a) RMS speckle contrast and ILS assuming ideal 0.33 numerical aperture system imaging 22-nm lines and spaces with disk illumination (partial coherence of 0.7) and assumed 75-pm roughness. (b) LER degradation factor relative to in focus position computed by normalizing the speckle contrast and inverse ILS, respectively.

Simply using the degradation terms in Fig.1, one can accurately predict LWR trends through focus. The LWR is expected to be proportional to the speckle contrast divided by the ILS. Figure 2 shows a comparison of the modeled LWR through focus and this ratio. The full LWR modeling is performed as described in the literature [4] and results show very good agreement. Thus speckle and ILS serve as very good metrics for the LWR degradation we are ultimately concerned with. These results also demonstrate the importance of defocus in the process and that appropriate levels of defocus must be considered when determining mask roughness requirements.

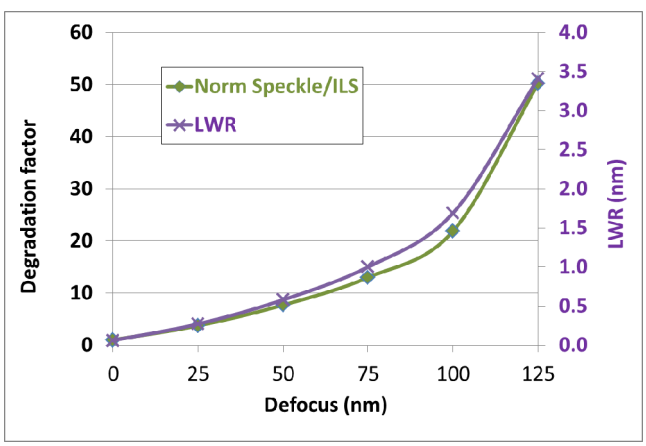

Fig. 2. Comparison of directly modeled LWR and speckle contrast to ILS ratio.

3. ROUGHNESS AS DEFECTIVITY

The first alternative specification perspective we consider is the most direct and relies simply on the notion that mask roughness can be viewed as a collection of random pit and bump defects. Given a statistical distribution for the roughness, we can then find the probability of any peak or valley within that distribution exceeding the defined phase defect specification. For example, considering the arbitrary rough surface in Fig. 3 which represents an RMS roughness of 100 pm, we see that within this small 0.8 μm × 0.8 μm area we already find a bump greater than 0.5-nm tall (circled).

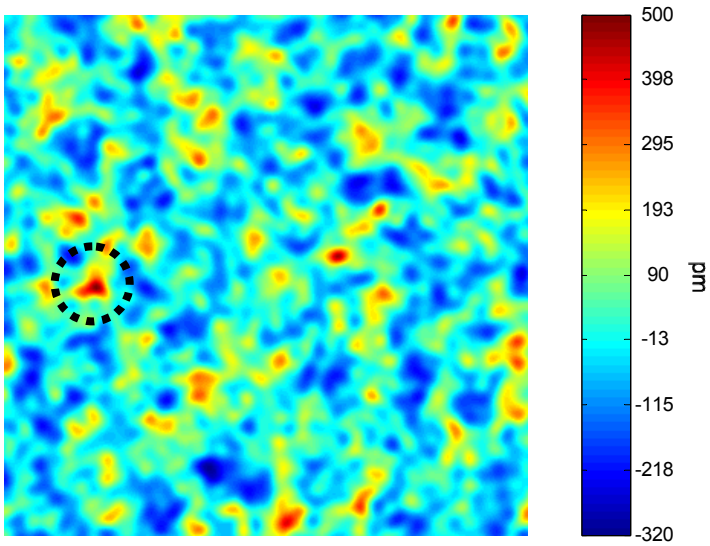

Fig. 3. 0.8 μm × 0.8 μm patch of rough surface with an RMS height variation of 100 pm. Within this small area we already find a bump greater than 0.5-nm tall (circled).

To determine the expected number of roughness induced defects on a mask we assume an active mask area of 140 mm × 110 mm and a correlation width of 80 nm in mask coordinates as determined by EUV-based scattering characterization of SEMATECH-provided mask blanks and assume Gaussian statistics for the roughness height. Taking the ratio of these areas yields an estimate of the total number of independent potential defect sites on the mask. Table 1 shows the resulting expected defect count per mask as a function of mask roughness and specified defect height limit. From this analysis, assuming a tolerable defect height of 0.5 nm, we can tolerate up to approximately 90 pm of mask roughness.

Table 1. Expected roughness-induced defect count per mask as a function of mask roughness (RSR) and target defect height.

	Printable defect height (nm)			
RSR (pm)	0.3	0.4	0.5	0.6
50	6.59E-05	3.44E-17	6.40E-33	4.16E-52
55	3.74E-02	2.52E-12	2.42E-25	3.26E-41
60	4.71E+00	1.28E-08	1.43E-19	6.40E-33
65	2.05E+02	9.92E-06	4.47E-15	1.84E-26
70	4.15E+03	1.96E-03	1.67E-11	2.48E-21
80	3.48E+05	4.71E+00	2.96E-06	8.51E-14
90	7.44E+06	1.00E+03	1.21E-02	1.28E-08
100	6.77E+07	4.72E+04	4.71E+00	6.59E-05
110	3.52E+08	8.30E+05	3.95E+02	3.74E-02
120	1.25E+09	7.44E+06	1.17E+04	4.71E+00
130	3.37E+09	4.14E+07	1.64E+05	2.05E+02

4. PATTERNED MASK INSPECTION

Next we consider the case of patterned mask inspection. As discussed above, mask roughness on a patterned mask leads to LWR and depending on the magnitude of the LWR, it may lead to critical dimension (CD) variations exceeding the specified defect tolerance and be flagged as a defect. Following the method used in Section 3, we determine the expected number of roughness induced defects on a patterned mask assuming an active mask area of 140 mm × 110 mm and a correlation width of 80 nm in mask coordinates. Gaussian statistics are assumed for the roughness induced LWR and we further assume the presence of 0.3-nm LWR (wafer coordinates) due to mask pattern LWR. The roughness and pattern induced LWR terms are assumed to be uncorrelated and thus to add in quadrature. Table 2 shows the expected defect count per mask as a function of mask roughness and specified critical dimension uniformity (CDU) requirement. Also shown in the table is the amount of roughness-induced LWR corresponding to each roughness value. In determining the LWR from the roughness, we assume an inspection NA of 0.17, disk illumination with a partial coherence of 0.5, and 1 Rayleigh unit of defocus. For a CDU requirement of 10%, we can only tolerate only up to approximately 45 pm of mask roughness, at a CDU requirement of 20%, the value increases to approximately 100 pm.

Table 2. Expected roughness-induced defect count per mask in patterned mask inspection as a function of mask roughness (RSR) and target CDU. Inspection imaging conditions: NA = 0.17, partial coherence = 0.5, defocus = 1 Rayleigh unit

		CDU Requirement	
RSR (pm)	Speckle LWR (nm)	10%	20%
20	0.16	2.81E-08	4.00E-63
30	0.24	2.77E-04	2.65E-47
44	0.35	7.39E+00	7.93E-30
56	0.45	4.37E+03	6.15E-19
69	0.55	3.40E+05	1.50E-11
81	0.65	6.89E+06	1.77E-06
94	0.75	5.83E+07	6.59E-03
106	0.85	2.77E+08	2.53E+00
119	0.95	8.90E+08	2.09E+02

4. DARKFIELD MASK BLANK INSPECTION

Next we consider darkfield mask blank inspection [10, 11]. In this case, the mask roughness again leads to speckle, but the final recorded speckle is at significantly lower contrast due to the camera pixel size being considerably larger than the speckle size. Nevertheless, given the imaging and detection conditions, the image speckle can be determined and compared to the expected defect signal. Again using the method above, we determine the expected number of roughness induced defects on a mask blank assuming an active mask area of 140 mm × 110 mm and a detection noise correlation width of 519 nm in mask coordinates. This is determined from an assumed detector CCD pixel size of 13.5 mm and an optical magnification of 26×. Since the actual speckle size is much smaller than the imaged pixel size, the pixel size determines the effective correlation length. In computing the speckle and defect sensitivity, we assume an outer NA of 0.2, an inner NA (central obscuration) of 0.1, a partial coherence of 0.5 (illumination just fills the central obscuration) as well as the magnification and pixel size quoted above. Note that in darkfield mode, the imaging characteristics are quite insensitive to defocus. Table 3 shows the expected defect count per mask as a function of mask roughness and target defect height. Achieving a defect sensitivity of 0.6 nm requires the roughness to be smaller than approximately 50 pm.

Table 3. Expected roughness-induced defect count per mask in patterned mask inspection as a function of mask roughness (RSR) and target defect height. Inspection imaging conditions: $NA_{out} = 0.2$, $NA_{in} = 0.1$, partial coherence = 0.5, magnification = 26×, pixel size = 13.5 μm.

	Target defect height (nm)			
RSR (pm)	0.4	0.6	0.8	1.0
50	5.28E+06	8.00E-08	2.22E-44	3.90E-121
60	3.79E+08	5.72E+01	1.01E-16	7.75E-54
70	2.63E+09	4.10E+05	8.39E-05	6.37E-25
80	7.24E+09	3.37E+07	5.72E+01	7.71E-11
90	1.30E+10	3.79E+08	7.92E+04	2.64E-03
100	1.88E+10	1.59E+09	5.28E+06	5.72E+01
110	2.40E+10	3.95E+09	7.04E+07	2.54E+04
120	2.84E+10	7.24E+09	3.79E+08	1.26E+06

5. MEASURING EUV ROUGHNESS

To date, characterization of mask roughness has typically been based on atomic force microscopy (AFM) of either the substrate or the coating. Unfortunately, neither of these metrics are strictly representative of the true EUV roughness which depends in large part on the roughness within the multilayer and how this roughness is correlated from layer to layer, especially in the top 10 or so bilayers which contribute to the majority of the reflectivity. For example in Ref. [7], full 3D modeling demonstrated that the depending on the specifics of the roughness evolution through the multilayer stack, the resulting worst-case speckle could vary by as much as a factor of 4.

The deviation between AFM and EUV scattering (XRS) based characterization has been documented in the literature [12] and an example of this deviation is shown in Fig. 4 which compares substrate AFM results to x-ray scattering results. Depending on the starting roughness, we see errors as large as 100%.

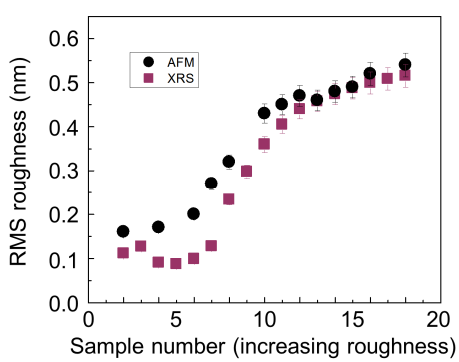

Fig. 4. Direct comparison of AFM measured substrate roughness and EUV roughness as determined by EUV scattering (XRS) measurements.

Even more insight can be obtained by comparison of the full roughness power spectrum as shown in Fig. 5. These results were obtained from commercially supplied EUV mask substrates coated by SEMATECH in Albany NY. The AFM results include both characterization of the substrate prior to coating as well as the top surface of the multilayer after coating. We show the results for two different blanks: in one case the EUV roughness is considerably smaller than both the substrate and multilayer AFM results whereas in a second case the EUV roughness lies between the two AFM measurements. Again it is evident that AFM based results are not representative of the EUV roughness and that the error furthermore varies with spatial frequency.

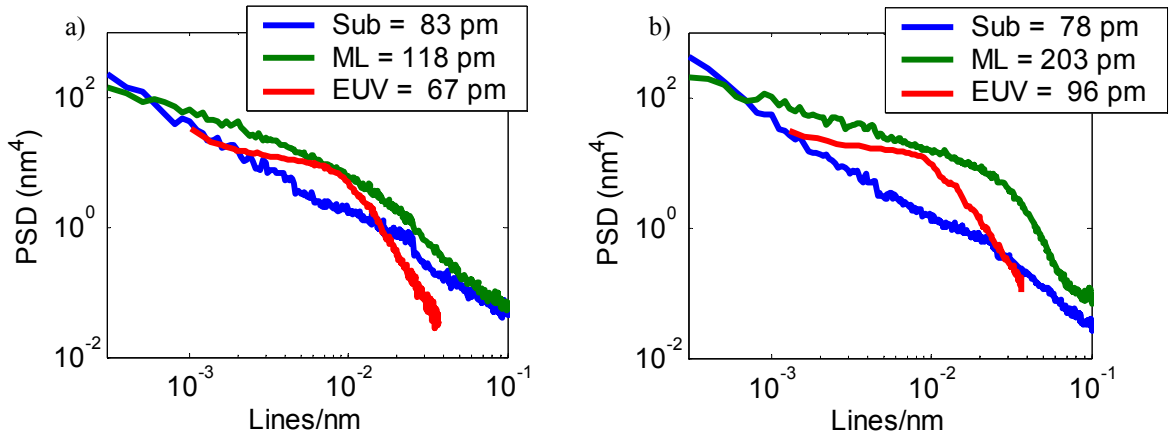

Fig. 5. Direct comparison of the roughness power spectral density (PSD) for three different measurement methods: 1) AFM of the substrate (Sub), AFM of the multilayer (ML), and EUV scatterometry (EUV). The results are from results commercially supplied EUV mask substrates coated by SEMATECH in Albany NY. The numbers reported in the legends represent the total measured RMS roughness.

5. AERIAL IMAGE VERIFICATION

The mask roughness requirements reported here and earlier rely on the validity of the speckle modeling [8]. This validity has been lithographically demonstrated in the past, but only with very rough masks and extreme imaging conditions allowing the intrinsic resist LER to be overwhelmed [13]. To test more realistic roughness and imaging conditions today, however, we cannot rely on resists, but rather need to use EUV microscopy tools such as SHARP [14] and SERM [15]. The first example we consider is the SHARP-based measurement of EUV clear field speckle of the mask blank shown in Fig. 5(a). The results in Fig. 6 show the speckle as a function of focus for two different coherence settings. The plots show both the SHARP-measured RMS speckle contrast as well as the computed speckle contrast. The computed values are determined using the EUV scattering based roughness measurement described above. Slight discrepancies can be observed, but overall the agreement is quite good. We attribute the errors to possible aberrations in the tool and/or illumination alignment errors.

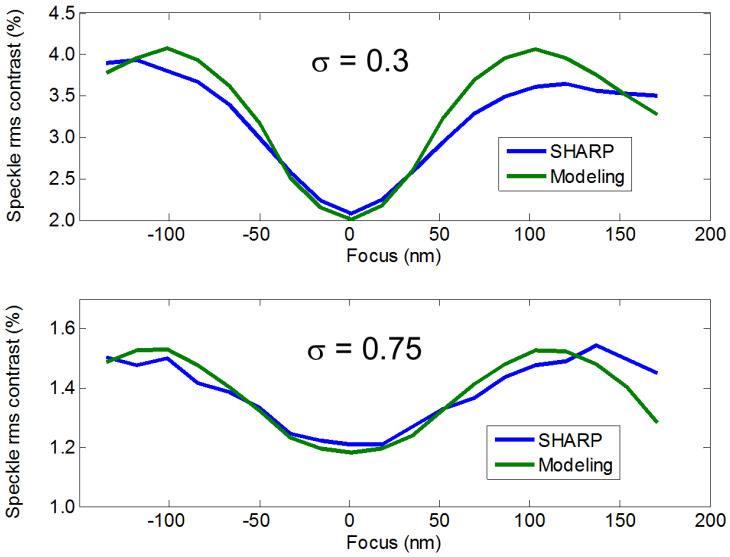

Fig. 6. SHARP-based measurement of EUV clear field speckle of mask blank in Fig. 5(a). Plots show speckle as a function of focus for two different coherence settings: both SHARP-measured RMS speckle contrast and computed speckle contrast are shown. Computation is based on the scattering roughness measurement described above.

The next example we consider is the SERM-based measurement of LWR for a commercially supplied mask. The SERM microscope is an EUV scanning probe microscope using zoneplate optics fabricated at the Center for X-ray Optics [16] and a standalone commercial EUV high harmonic source [17]. We measure 22-nm lines and spaces (1×) using an effective NA of 0.33 and a partial coherence of 0.9. To mitigate the effect of noise and help extract the small roughness-induced LWR, we apply the repeated measurement correlation technique [13]. Figure 7 shows the results from the correlation measurement from which the mask-induced LWR (LWR_{mask}) can be determined using the equation

$$LWR_{mask} = R \times LWR_{meas} \qquad (1)$$

where R is the linear correlation coefficient and LWR_{meas} is the total measured LWR. From the results in Fig. 7, we determine the mask-induced LWR to be 1.60 nm from which we subtract the expected pattern contribution of 1.48 nm in quadrature, yielding a roughness-induced LWR of 0.62 nm. This compares quite well to the predicted LWR of 0.60 nm based on the measured roughness characteristics of the mask.

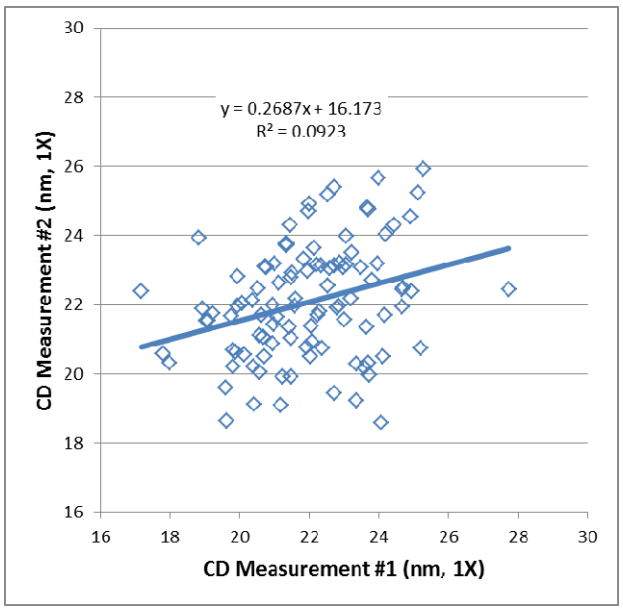

Fig. 7. SERM-based measurement of LWR for commercially supplied mask. Results are for 22-nm lines and spaces (1×) using an effective NA of 0.33 and a partial coherence of 0.9. The two-measurement method yields a Coefficient of Determination (R^2) of 0.0923

6. SUMMARY

The limits on EUV mask multilayer roughness have been investigated from a variety of perspectives related to mask inspection and defectivity. The analysis leads to roughness requirements in the 50 to 100 pm range and is consistent with previously presented lithographic analysis [6].

The characterization of mask roughness has also been studied, demonstrating a significant discrepancy between AFM results and true EUV roughness as measured by actinic scattering. This is true for AFM of either the substrate or the multilayer top surface.

This work was funded in part by SEMATECH and we acknowledge Kevin Cummings, Dominic Ashworth, and Anne Rudack for programmatic support. Student support for this work was provided by IMPACT+ (Integrated Modeling Process and Computation for Technology). Member companies – Applied Materials, ARM, ASML, Global Foundries, IBM, Intel, KLA-Tencor, Marvell Technology, Mentor Graphics, Panoramic Tech, Photronics, Qualcomm, Samsung, SanDisk and Tokyo Electron. Measurements performed on the SHARP EUV microscope were funded by SEMATECH and conducted by the Center for X-Ray Optics at the Lawrence Berkeley National Laboratory Advanced Light Source synchrotron radiation facility. The Advanced Light Source is supported by the Director, Office of Science, Office of Basic Energy Sciences, of the U.S. Department of Energy under Contract No. DE-AC02-05CH11231.

REFERENCES

1. Martin Lowisch, Peter Kuerz, Olaf Conradi, Gero Wittich, Wolfgang Seitz, Winfried Kaiser, "Optics for ASML's NXE:3300B platform," Proc. of SPIE **8679**, 86791H (2013).
2. N. Beaudry, T. Milster, "Effects of mask roughness and condenser scattering in EUVL systems," Proc. SPIE. **3676**, 653-662 (1999).
3. P. Naulleau, "The relevance of mask-roughness-induced printed line-edge roughness in recent and future EUV lithography tests," Appl. Opt. **43**, 4025-4032 (2004).
4. P. Naulleau, D. Niakoula, G. Zhang, "System-level line-edge roughness limits in extreme ultraviolet lithography," J. Vac. Sci. & Technol. B **26**, 1289-1293 (2008).
5. http://www.itrs.net/Links/2013ITRS/Summary2013.htm
6. P. Naulleau and S. George, "Implications of image plane line-edge roughness requirements on extreme ultraviolet mask specifications," Proc. SPIE **7379**, 73790O-73790O-11 (2009).
7. P. Naulleau and S. George, "Validity of the thin mask approximation in extreme ultraviolet mask roughness simulations," Appl. Opt., **50**, 3346 (2011).
8. P. Naulleau, B. McClinton, K. Goldberg, I. Mochi, A. Rastegar, "Mask roughness challenges in extreme ultraviolet mask development," J. Vac. Sci. & Technol. B **29**, 06F501 (2011).
9. H. Levinson, Principles of lithography, Chapt. 2, SPIE, Bellingham WA, 2005.
10. T. Yamane, T. Tanaka, T. Terasawa, O. Suga, "Improvement of actinic blank inspection and phase defect analysis," Proc. SPIE **7823**, 1 – 8 (2010).
11. T. Yamane, T. Tanaka, T. Terasawa, O. Suga, "Phase defect analysis with actinic full-field EUVL mask blank inspection," Proc. SPIE **8166**, 81660G 1 – 8 (2011).
12. S. George, P. Naulleau, I. Mochi, F. Salmassi, E. Gullikson, K. Goldberg, E. Anderson, "Replicated mask surface roughness effects on EUV lithographic patterning and line-edge roughness," Proc. SPIE **7969**, 79690E (2011).
13. P. Naulleau, "Correlation method for the measure of mask-induced line-edge roughness in extreme ultraviolet lithography," Appl. Opt. **48**, 3302-3307 (2009).
14. K. Goldberg, M. Benk, A. Wojdyla, I. Mochi, S. Rekawa, A. Allezy, M. Dickinson, C. Cork, W. Chao, D. Zehm, J. Macdougall, P. Naulleau, A. Rudack, "Actinic mask imaging: Recent results and future directions from the SHARP EUV Microscope," Proc. SPIE **9048**, 90480Y-1 (2014).
15. S. Kim, D. Lee, J. Park, E. Kim, C. Jeon, H. Cho, B. Jeon, C. choi, C. Anderson, R. Myakawa, P. Naulleau, "EUV mask imaging system based on the scanning reflective microscopy," 2013 International Symposium on Extreme Ultraviolet Lithography, Toyama, Japan, October 6-10, 2013, proceedings available from SEMATECH, Albany, NY.
16. http://cxro.lbl.gov/nanofabrication
17. B. Yoo, "EUVO: EUV Light Generation System," 2013 International Symposium on Extreme Ultraviolet Lithography, Toyama, Japan, October 6-10, 2013, proceedings available from SEMATECH, Albany, NY.